ELSEVIER

Journal of Hazardous Materials B137 (2006) 384–395

Journal of Hazardous Materials

www.elsevier.com/locate/jhazmat

Removal of copper(II) and lead(II) from aqueous solution by manganese oxide coated sand I. Characterization and kinetic study

Runping Han [a,*], Weihua Zou [a], Zongpei Zhang [a], Jie Shi [a], Jiujun Yang [b]

[a] *Department of Chemistry, Zhengzhou University, No. 75 of Daxue North Road, Zhengzhou 450052, PR China*

[b] *College of Material Science and Engineering, Zhengzhou University, No. 75 of Daxue North Road, Zhengzhou 450052, PR China*

Received 8 November 2005; received in revised form 25 December 2005; accepted 13 February 2006

Available online 28 February 2006

Abstract

The preparation, characterization, and sorption properties for Cu(II) and Pb(II) of manganese oxide coated sand (MOCS) were investigated. A scanning electron microscope (SEM), X-ray diffraction spectrum (XRD) and BET analyses were used to observe the surface properties of the coated layer. An energy dispersive analysis of X-ray (EDAX) and X-ray photoelectron spectroscopy (XPS) were used for characterizing metal adsorption sites on the surface of MOCS. The quantity of manganese on MOCS was determined by means of acid digestion analysis. The adsorption experiments were carried out as a function of solution pH, adsorbent dose, ionic strength, contact time and temperature. Binding of Cu(II) and Pb(II) ions with MOCS was highly pH dependent with an increase in the extent of adsorption with the pH of the media investigated. After the Cu(II) and Pb(II) adsorption by MOCS, the pH in solution was decreased. Cu(II) and Pb(II) uptake were found to increase with the temperature. Further, the removal efficiency of Cu(II) and Pb(II) increased with increasing adsorbent dose and decreased with ionic strength. The pseudo-first-order kinetic model, pseudo-second-order kinetic model, intraparticle diffusion model and Elovich equation model were used to describe the kinetic data and the data constants were evaluated. The pseudo-second-order model was the best choice among all the kinetic models to describe the adsorption behavior of Cu(II) and Pb(II) onto MOCS, suggesting that the adsorption mechanism might be a chemisorption process. The activation energy of adsorption (E_a) was determined as Cu(II) 4.98 kJ mol^{-1} and Pb(II) 2.10 kJ mol^{-1}, respectively. The low value of E_a shows that Cu(II) and Pb(II) adsorption process by MOCS may involve a non-activated chemical adsorption and a physical sorption.

Keywords: Manganese oxide coated sand (MOCS); Cu(II); Pb(II); Adsorption kinetic

1. Introduction

The presence of heavy metals in the aquatic environment is a major concern due to their extreme toxicity towards aquatic life, human beings, and the environment. Heavy metal ions from wastewaters are commonly removed by chemical precipitation, ion-exchange, reverse osmosis processes, and adsorption by activated carbon. Over the last few decades, adsorption has gained importance as an effective purification and separation technique used in wastewater treatment, and the removal of heavy metals from metal-laden tap or wastewater is considered an important application of adsorption processes using a suitable adsorbent [1,2].

In recent years, many researchers have applied metal oxides to adsorption of heavy metals from metal-laden tap or wastewater [3]. Adsorption can remove metals over a wider pH range and lower concentrations than precipitation [4]. Iron, aluminum, and manganese oxides are typically thought to be the most important scavengers of heavy metals in aqueous solution or wastewater due to their relatively high surface area, microporous structure, and possess OH functional groups capable of reacting with metals, phosphate and other specifically sorbing ions [5]. However, most metal oxides are available only as fine powders or are generated in aqueous suspension as hydroxide floc or gel. Under such conditions, solid/liquid separation is fairly difficult. In addition, metal oxides along are not suitable as a filter medium because of

* Corresponding author. Tel.: +86 371 67763707; fax: +86 371 67763220.
E-mail address: rphan67@zzu.edu.cn (R. Han).

0304-3894/$ – see front matter © 2006 Elsevier B.V. All rights reserved.
doi:10.1016/j.jhazmat.2006.02.021

their low hydraulic conductivity. Recently, several researchers have developed techniques for coating metal oxides onto the surface of sand to overcome the problem of using metal oxides powers in water treatment. Many reports have shown the importance of these surface coatings in controlling metal distribution in soils and sediments [3,6,7].

In recent years, coated minerals have been studied because of their potential application as effective sorbents [3,8,9]. Iron oxide coated meterials for heavy metal removal have been proved successful for the enhancement of treatment capacity and efficiency when compared with uncoated filter media, such as silica sand [10–14], granular activated carbon [15] and polymeric media [16,17]. For example, Edwards and Benjamin [7] found that coated media have similar properties to unattached coating materials in removing metals over a wide pH range, and that Fe oxide coated sand was more effective than uncoated sand. Bailey et al. [18] used iron oxide coated sand to remove hexavalent chromium from a synthetic waste stream. The influent contained 20 mg l^{-1} Cr(VI) and better than 99% removal was achieved. Satpathi and Chaudhuri [19] and Viraraghavan et al. [20] have recently reported on the ability of this medium to adsorb metals from electroplating rinse waters and arsenic from drinking water sources, respectively. Green-Pedersen and Pind reported that a ferrihydrite-coated montmorillonite surface had a larger specific surface area and an increased sorption capacity for Ni(II) compared to the pure systems [21]. Meng and Letterman [22] found that the adsorption properties of oxide mixtures are determined by the relative amount of the components. They also found that ion adsorption on aluminum oxide-coated silica was better modeled assuming uniform coverage of the oxide rather than using two distinct surfaces [23]. Lo and Chen [8] determined the effect of Al oxide mineralogy, amount of oxide coating, and acid- and alkali-resistance on the removal of selenium from water. Brandao and Galembecket reported that the impregnation of cellulose acetates with manganese dioxide resulted in high removal efficient of Cu(II), Pb(II), and Zn(II) from aqueous solutions [24]. Al-Degs and Khraisheh [25] also reported that diatomite and manganese oxide modified diatomite are effective adsorbents for removing Pb^{2+}, Cu^{2+}, and Cd^{2+} ions. The sorption capacity of Mn-diatomite was considerably increased compared to the original material for removing the studied metals. Filtration quality of diatomite is significantly increased after modification with Mn-oxides. Merkle et al. [26–28] reported that manganese dioxide coated sand was effective for removal of arsenic from ground water in column experiments. Merkle et al. developed a manganese oxide coating method on anthracite to improve the removal of Mn^{2+} from drinking water and hazardous waste effluent. They generated a filter media with an increased surface area after coating with manganese oxides and found manganese oxide coated media have the ability to adsorb and coprecipitate a variety of inorganic species. Stahl and James [29] found their manganese oxide coated sands generated a larger surface area and increased adsorption capability with increasing pH as compared to uncoated silica sand.

Additional researchers have been investigated to evaluate coating characteristics. X-ray diffraction (XRD), X-ray photoelectron spectroscopy (XPS), Fourier transform infrared spectroscopy (FTIR), transmission electron microscopy (TEM), and scanning electron microscopy (SEM) have been used as well to identify components, distribution, and structure of surface oxide coating [7,9,30,31]. An energy dispersive X-ray (EDAX) technique of analysis has been used to characterize metal adsorption sites on the sorbent surface. Typically, oxide was non-uniform over the surface as both the oxide and substratum had been observed [7].

The research described here was designed to investigate characteristics of manganese oxide coated sand (MOCS) and test the properties of MOCS as an adsorbent for removing copper (II) and lead (II) from synthetic solutions in batch system. SEM/EDAX, XRD, XPS and BET analysis were employed to examine the properties of adsorption reactions for Cu(II) and Pb(II) ions on MOCS in water. The system variables studied include pH, MOCS dose, ionic strength, contact time and temperature. The kinetic parameters, such as E_a, k_1, k_2, have been calculated to determine rate constants and adsorption mechanism.

1.1. Kinetic parameters of adsorption

The models of adsorption kinetics were correlated with the solution uptake rate, hence these models are important in water treatment process design. In order to analyze the adsorption kinetics of MOCS, four kinetic models including the pseudo-first-order equation [32], the pseudo-second-order equation [33], Elovich equation [34], and intraparticle diffusion model [35] were applied to experimental data obtained from batch metal removal experiments.

A pseudo-first-order kinetic model of Lagergen is given as

$$\log(q_e - q_t) = \log\, q_e - \frac{K_1 t}{2.303} \tag{1}$$

A pseudo-second-order kinetic model is

$$\frac{t}{q_t} = \frac{1}{(K_2 q_e^2)} + \frac{t}{q_e} \tag{2}$$

and

$$h = K_2 q_e^2 \tag{3}$$

an intraparticle diffusion model is

$$q_t = K_t t^{1/2} + C \tag{4}$$

and an Elovich equation model is shown as

$$q_t = \frac{\ln(\alpha\beta)}{\beta} + \frac{\ln\, t}{\beta} \tag{5}$$

where q_e and q_t are the amount of solute adsorbed per unit adsorbent at equilibrium and any time, respectively (mmol g^{-1}), k_1 the pseudo-first-order rate constant for the adsorption process (min^{-1}), k_2 the rate constant of pseudo-second-order adsorption (g $mmol^{-1}$ min^{-1}), K_t the intraparticle diffusion rate constant (mmol g^{-1} min^{-1}), h the initial sorption rate of pseudo-second-order adsorption (mmol g^{-1} min^{-1}), C the intercept, α the initial sorption rate of Elovich equation (mmol g^{-1} min^{-1}), and

the parameter β is related to the extent of surface coverage and activation energy for chemisorption (g mmol^{-1}). A straight line of $\log(q_e - q_t)$ versus t, t/q_t versus t, q_t versus $\ln t$, or q_t versus $t^{1/2}$ suggests the applicability of this kinetic model and kinetic parameters can be determined from the slope and intercept of the plot.

1.2. Determination of thermodynamic parameters

The activation energy for metal ions adsorption was calculated by the Arrhenius equation [36]:

$$k = k_0 \exp\left[\frac{-E_a}{RT}\right] \quad (6)$$

where k_0 is the temperature independent factor in g mmol^{-1} min^{-1}, E_a the activation energy of the reaction of adsorption in kJ mol^{-1}, R the gas constant (8.314 J mol^{-1} K^{-1}) and T is the adsorption absolute temperature (K). The linear form is:

$$\ln k = \frac{-E_a}{RT} + \ln k_0 \quad (7)$$

when $\ln k$ is plotted versus $1/T$, a straight line with slope $-E_a/R$ is obtained.

2. Materials and methods

2.1. Adsorbent

The quartz sand was provided from Zhengzhou's Company of tap water in China. The diameter of the sand was ranged in size from 0.99 to 0.67 mm. The sand was soaked in 0.1 mol l^{-1} hydrochloric acid solution for 24 h, rinsed with distilled water and dried at 373 K in the oven in preparation for surface coating. Manganese oxide coated sand was accomplished by utilizing a reductive procedure modified to precipitate colloids of manganese oxide on the media surface. A boiling solution containing potassium permanganate was poured over dried sand placed in a beaker, and hydrochloric acid (37.5%, W_{HCl}/W_{H_2O}) solution was added dropwise into the solution. After stirring for 1 h, the media was filtered, washed to pH 7.0 using distilled water, dried at room temperature, and stored in polypropylene bottle for future use.

2.2. Metal solutions

All chemicals and reagents used for experiments and analyses were of analytical grade. Stock solutions of 2000 mg l^{-1} Pb(II) and Cu(II) were prepared from $Cu(NO_3)_2$ and $Pb(NO_3)_2$ in distilled, deionized water containing a few drops of concentrated HNO_3 to prevent the precipitation of Cu(II) and Pb(II) by hydrolysis. The initial pH of the working solution was adjusted by addition of HNO_3 or NaOH solution.

2.3. Mineral identification

The mineralogy of the sample was characterized by X-ray diffraction (XRD) (Tokyo Shibaura Model ADG-01E). Photomicrography of the exterior surface of uncoated sand and manganese oxide coated sand was obtained by SEM (JEOL6335F-SEM, Japan). The distribution of elemental concentrations for the solid sample can be analyzed using the mapping analysis of SEM/EDAX (JEOL SEM (JSM-6301)/OXFORD EDX, Japan). The existence of Cu(II) and Pb(II) ions on the surface of manganese oxide coated sand was also confirmed by using EDAX. Samples for EDAX analysis were coated with thin carbon film in order to avoid the influence of any charge effect during the SEM operation. The samples of MOCS and MOCS adsorbed with copper/lead ions were also analyzed by X-ray photoelectron spectroscopy (XPS) (ESCA3600 Shimduz).

2.4. Specific surface area and pore size distribution analyses

Analyses of physical characteristics of MOCS included specific surface area, and pore size distributions. The specific surface area of MOCS and pore volumes were test using the nitrogen adsorption method with NOVA 1000 High-Speed, Automated Surface Area and Pore Size Analyer (Quantachrome Corporation, America) at 77 K, and the BET adsorption model was used in the calculation. Calculation of pore size followed the method of BJH according to implemented software routines.

2.5. Methods of adsorption studies

Batch adsorption studies were conducted by shaking the flasks at 120 rpm for a period of time using a water bath cum mechanical shaker. Following a systematic work on the sorption uptake capacity of Cu(II) and Pb(II) in batch systems were studied in the present work.

The experimental process was as following: put a certain quantity of MOCS into conical flasks, then, added the solute of metals of copper or lead in single component system, vibrated sometime at a constant speed of 120 rpm in a shaking water bath, when reached the sorption equilibrium after 180 min, took out the conical flasks, filtrated to separate MOCS and the solution. No other solutions were provided for additional ionic strength expect for the effect of ionic strength. The concentration of the free metal ions in the filtrate was analyzed using flame atomic absorption spectrometer (AAS) (Aanalyst 300, Perkin Elmer). The uptake of the metal ions was calculated by the difference in their initial and final concentrations. Effect of pH (1.4–6.5), quantity of MOCS, contact time, temperature (288–318 K) was studied. The pH of the solutions at the beginning and end of experiments was measured. Each experiment was repeated three times and the results given were the average values.

2.5.1. Effect of contact time and temperature on Cu(II) and Pb(II) adsorption

A 2.0 g l^{-1} sample of MOCS was added to each 20 ml of Cu(II) or Pb(II) solutions with initial concentration of Cu(II) 0.315 mmol l^{-1} and Pb(II) 0.579 mmol l^{-1}, respectively. The temperature was controlled with a water bath at the temperature ranged from 294 to 318 K for the studies. Adsorbent of MOCS and metal solution were separated at pre-determined time inter-

vals, filtered and analyzed for residual Cu(II) and Pb(II) ion concentrations.

2.5.2. Effect of pH on the sorption of Cu(II) and Pb(II) by MOCS

The effect of pH on the adsorption capacity of MOCS was investigated using solutions of 0.157 mmol l^{-1} Cu(II) and 0.393 mmol l^{-1} Pb(II) for a pH range of 1.4–6.5 at 293 K. A 20 g l^{-1} of MOCS was added to 20 ml of Cu(II) and Pb(II) solutions. Experiments could not be performed at higher pH values due to low solubility of metal ions.

2.5.3. Effect of MOCS dose

It was tested by the addition of sodium nitrate and calcium nitrate to the solution of Cu(II) and Pb(II), respectively. The dose of adsorbents were varied from 10 to 80 g l^{-1} keeping initial concentration of copper 0.157 mmol l^{-1} and lead 0.393 mmol l^{-1}, respectively, and contact time was 180 min at the temperature of 293 K.

2.5.4. Effect of ionic strength on Cu(II) and Pb(II) adsorption

The concentration of $NaNO_3$ and $Ca(NO_3)_2$ used ranged from 0 to 0.2 mol l^{-1}. The dose of adsorbents were 20 g l^{-1}, the initial concentration of copper 0.157 mmol l^{-1} and lead 0.393 mmol l^{-1}, respectively, and contact time was 180 min at the temperature of 293 K.

The data obtained in batch model studies was used to calculate the equilibrium metal uptake capacity. It was calculated for each sample of copper by using the following expression:

$$q_t = \frac{v(C_0 - C_t)}{m} \quad (8)$$

where q_t is the amount of metal ions adsorbed on the MOCS at time t (mmol g^{-1}), C_0 and C_t the initial and liquid-phase concentrations of metal ions at time t (mmol l^{-1}), v the volume of the aqueous phase (l) and m is the dry weight of the adsorbent (g).

3. Results and discussion

3.1. Mineralogy of manganese oxide coated sand

The samples of sand coated with manganese oxide were dark colored (brown–black) precipitates, indicating the presence of manganese in the form of insoluble oxides. The X-ray diffraction spectrum (XRD) of the samples (data not shown) revealed that the manganese oxide were totally amorphous, as there was not any peak detected, indicative of a specific crystalline phase. SEM photographs in Fig. 1 were taken at 10,000× magnifications to observe the surface morphology of uncoated sand and manganese oxide coated sand, respectively. SEM images of acid-washed uncoated quartz sand in Fig. 1(a) showed very ordered silica crystals at the surface. The virgin sand had a relatively uniform and smooth surface and small cracks, micropores or light roughness could be found on the sand surface. Comparing the images of virgin (Fig. 1(a)) and manganese oxide coated sand (Fig. 1(b)), MOCS had a significantly rougher surface than plain sand and the coated sand surfaces were apparently occupied by newborn manganese oxides, which were formed during the coating process. Fig. 1(b) also showed manganese oxides, formed in clusters, apparently on occupied surfaces. At the micron scale, the synthetic coating was composed of small particles on top of a more consolidated coating. In most regions individual particles of manganese oxide (diameter = 2–3 μm) appeared to be growing in clumps in surface depressions and coating cracks. The amount of manganese on the surface of the MOCS, measured through acid digestion analysis, was approximately 5.46 mg Mn/g-sand.

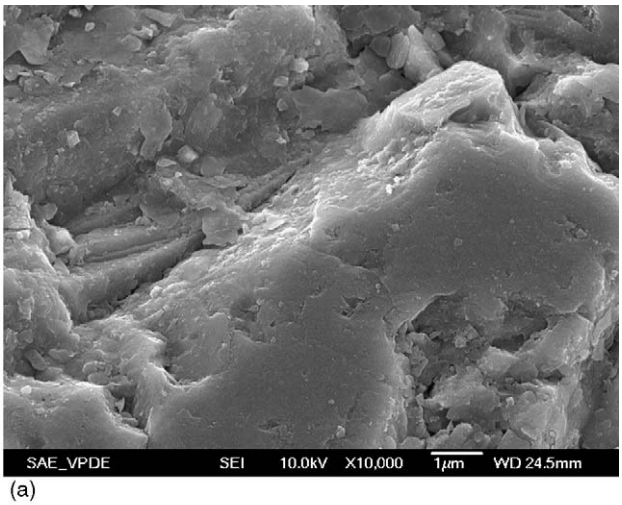

Fig. 1. SEM micrograph of sample: (a) sand; (b) manganese oxide coated sand.

3.2. SEM/EDAX analysis

The elements indicated as being associated with manganese oxide coated were detected by the energy dispersive X-ray spectrometer system (EDAX) using a standardless qualitative EDAX analytical technique. The peak heights in the EDAX spectra are proportional to the metallic elements concentration. The qualitative EDAX spectra for MOCS (Fig. 2(a)) indicated that Mn, O,

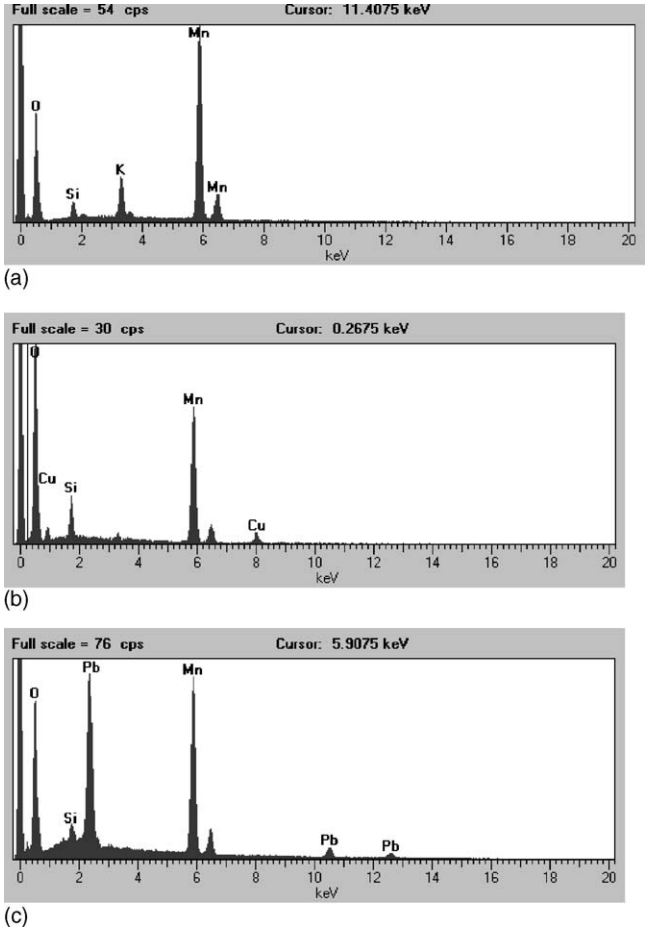

Fig. 2. EDAX spectrum of MOCS under: (a) adsorbed without copper and lead ion; (b) adsorbed copper ions; (c) adsorbed lead ions.

Si, and K are the main constituents. These had been known as the principal elements of MOCS. EDAX analysis yielded indirect evidence for the mechanism of manganese oxide on the surface of MOCS. The peak of Si occurred in EDAX showed that manganese oxides do not covered a full surface of the MOCS. If the solid sample of MOCS caused a change of elemental constitution through adsorption reaction, it could be inferred that manganese oxide has already brought about chemical interaction with adsorbate. The EDAX spectrum for copper and lead system was illustrated in Fig. 2(b and c). It could be seen that copper and lead ion became one element of solid sample in this spectrum. The reason was that copper and lead ions were chemisorbed on the surface of MOCS.

Dot mapping can provide an indication of the qualitative abundance of mapping elements. The elemental distribution mapping of EDAX for the sample of MOCS and MOCS adsorbed copper or lead ions is illustrated in Fig. 3. The bright points represented the single of the element from the solid sample. A laryer of manganese oxide coating is clearly shown in the dot map for Mn in Fig. 3(a), and a high density of white dots indicates manganese is the most abundant element. Results indicated that manganese oxide was spread over the surface of MOCS, and was a constituent part of the solid sample. The element distribution mapping of EDAX for the sample of MOCS

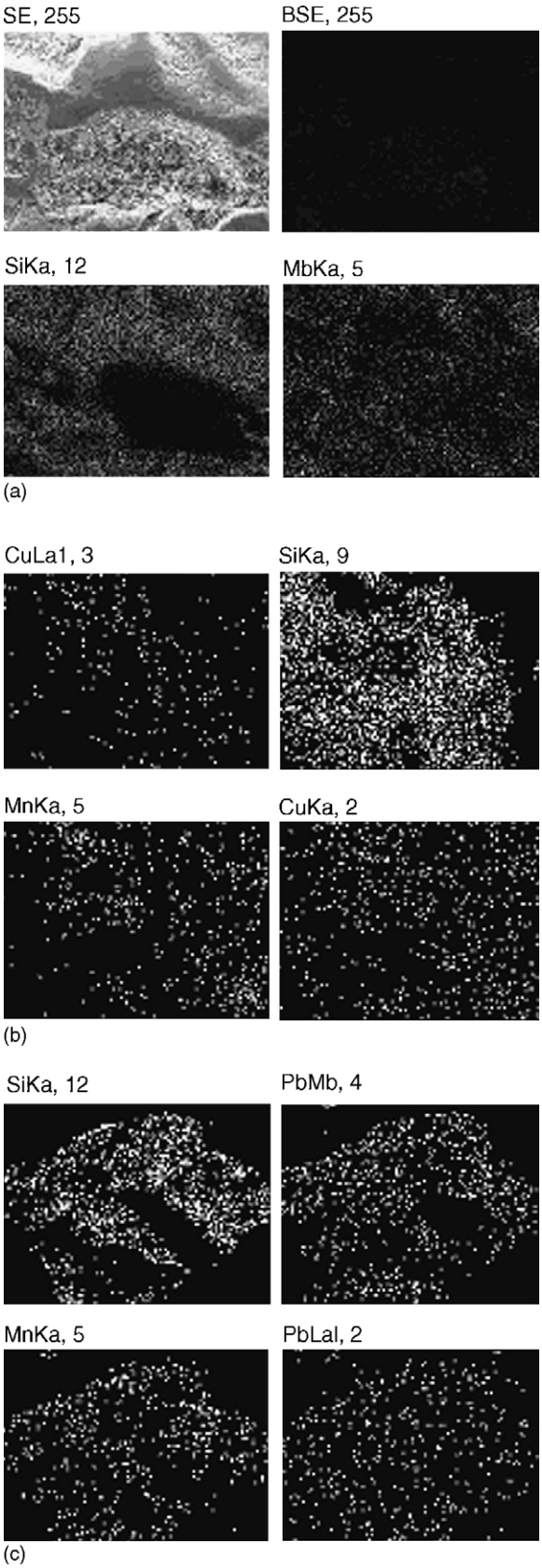

Fig. 3. EDAX results of MOCS (white images in mapping represent the corresponding element): (a) adsorbed without copper and lead ion; (b) adsorbed copper ions; (c) adsorbed lead ions.

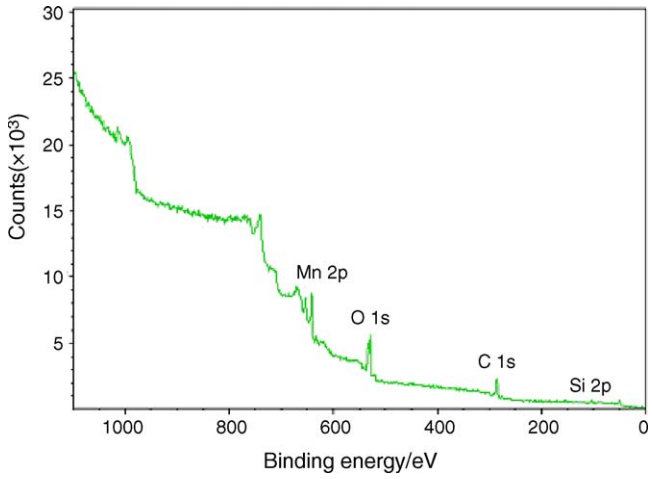

Fig. 4. XPS wide scan of the manganese oxide coated sand.

reacting with copper and lead ions is illustrated in Fig. 3(b and c). Copper or lead ions were spread over the surfaces of MOCS. Results indicated that manganese oxide produces chemical bond with copper or lead ions. Thus, copper or lead element was a constituent part of the solid sample.

3.3. Surface characterization using the X-ray photoelectron spectroscopy (XPS)

XPS analyses were performed on samples of MOCS alone and reacting with copper or lead ions. The wide scan of MOCS is presented in Fig. 4. It can be noticed that the major elements constituent are manganese, oxygen, and silicon. Detailed spectra of the peaks are shown in Fig. 5.

Manganese oxides are generally expressed with the chemical formula of MnO_x, due to the multiple valence states exhibited by Mn. Therefore, it is reasonable to measure the average oxidation state for a manganese mineral [37]. The observation of the Mn $2p_{3/2}$ peak at 641.9 eV and the separation between this and the Mn $2p_{1/2}$ peak of 11.4 eV indicates the manganese exhibited oxidation between Mn^{3+} and Mn^{4+} as shown from the auger plot, but it can be seen to show Mn^{4+} predominantly from the Mn $2p_{3/2}$ peaks [38].

The large peak in Fig. 5(b) is a sum of the two peaks at 529.3 and 533.1 eV, which can be assigned to O 1s; a low binding energy at 529.7 eV, which is generally accepted as lattice oxygen in the form of O^{2-} (metal oxygen bond). This peak is characteristic of the oxygen in manganese oxides. The second peak at 533.4 eV can be assigned to surface adsorbed oxygen in the form of OH^- [38].

As seen the XPS spectra of the sample of MOCS reacting with copper, Fig. 6(a) shows the binding energies of the observed photoelectron peaks of Cu $2p_{3/2}$, $2p_{1/2}$. The binding energy of the Cu $2p_{3/2}$ peak at a value of 933.9 eV shows the presence of copper (+2).

The XPS spectra obtained after Pb(II) adsorption on MOCS is presented in Fig. 6(b). Fig. 6(b) shows that doublets characteristic of lead appear, respectively, at 138.3 eV (assigned to Pb $4f_{7/2}$) and at 143.8 eV (assigned to Pb $4f_{5/2}$) after loading MOCS

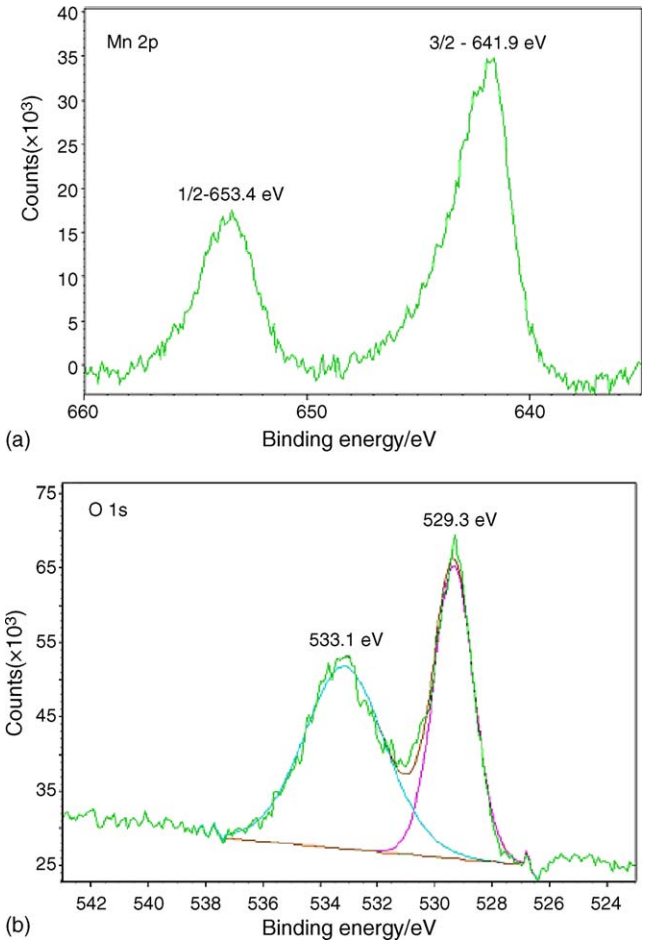

Fig. 5. XPS detailed spectra of MOCS: (a) Mn $2p_{3/2}$; (b) O 1s.

with Pb(II) solution. The peak observed at 138.3 eV agrees with the 138.0 eV value reported for PbO [39]. This shows a fixation of lead onto MOCS during the process.

3.4. Specific surface area and pore size distribution analyses

The specific surface areas for sand and MOCS under un/adsorbed Pb(II) ions are summarized in Table 1. Plain uncoated sand had a surface area of 0.674 $m^2\,g^{-1}$. A surface coating of manganese oxide increased the surface area of sand to 0.712 $m^2\,g^{-1}$, while average pore diameter decreased from 51.42 to 42.77 Å. This may be caused by the increase in both

Table 1
Specific surface areas and average pore diameters for sand and various MOCS

	Surface area ($m^2\,g^{-1}$)	Average pore diameter (Å)
Sand	0.674	51.42
Unadsorbed[a]	0.712	42.77
Adsorbed[b]	0.552	39.64
Desorbed[c]	0.701	42.71

[a] Without reacting with Pb(II) ions.
[b] After reacting with Pb(II) ions.
[c] After soaking with 0.5 mol l^{-1} acid solution.

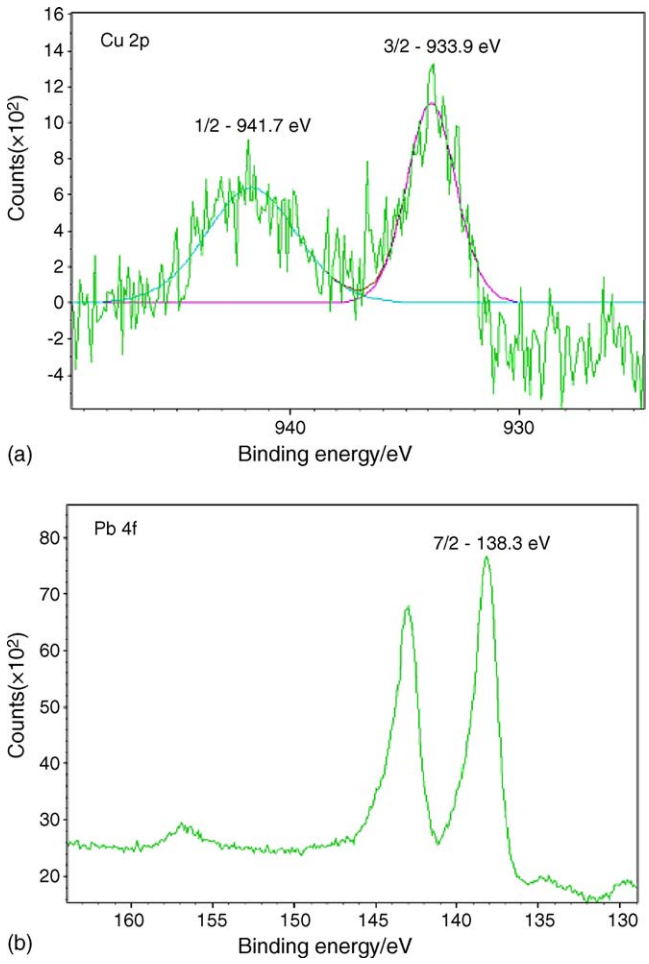

Fig. 6. XPS detailed spectra of MOCS reacting with (a) copper; (b) lead.

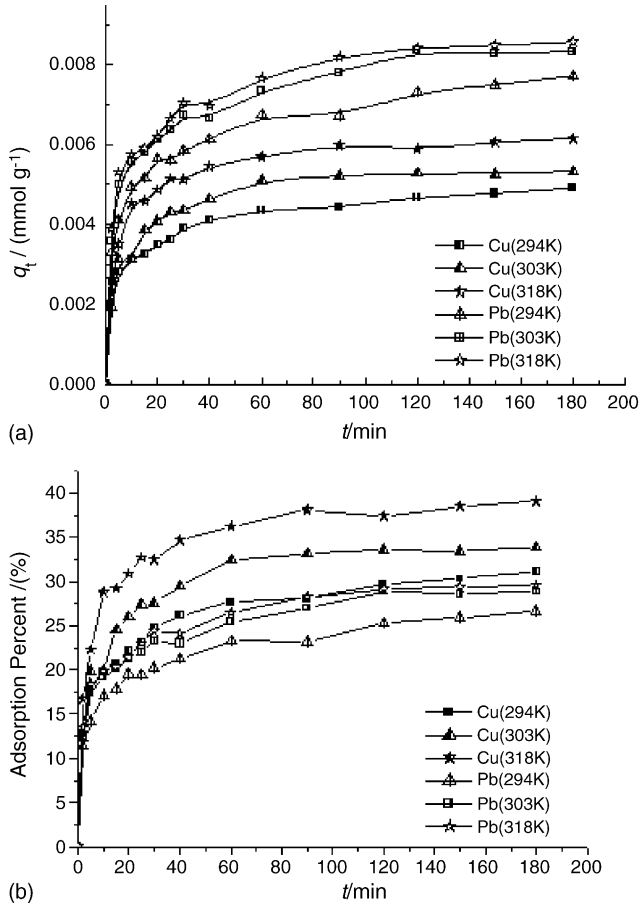

Fig. 7. Effect of contact time on Cu(II) and Pb(II) ions adsorption at pH 4 and various temperatures: (a) adsorption capacity vs. time; (b) adsorption percent vs. time ($C_{0(Cu)} = 0.315\,mmol\,l^{-1}$, $C_{0(Pb)} = 0.579\,mmol\,l^{-1}$).

inner and surface porosity after adding the manganese oxides admixture. After reacting with Pb(II) ions, the pore size distribution of MOCS had been changed, and parts of pores disappeared through the adsorption process. The results indicated the parts of pores were occupied with Pb(II) ions and average pore diameters decreased simultaneously, compared with unadsorbed MOCS, the surface area value of adsorbed MOCS is decreased, varying from of 0.712 to 0.552 $m^2\,g^{-1}$. Besides, pore size distribution of desorbed MOCS was similar to that of unadsorbed MOCS. The surface area of desorbed MOCS increased and average pore diameter also increased after regeneration with acid solution. The results indicated Pb(II) ions could be desorbed from the surface site of micropore and mesopores.

3.5. Effect of contact time and temperature on Cu(II) and Pb(II) adsorption

Effect of contact time and temperature on the adsorption of the copper(II) and lead(II) on MOCS was illustrated in Fig. 7(a and b). The uptake equilibrium of Cu(II) and Pb(II) were achieved after 180 min and no remarkable changes were observed for higher reaction times (not shown in Fig. 7). The shapes of the curves representing metal uptake versus time suggest that a two-step mechanism occurs. The first portion indicates that a rapid adsorption occurs during the first 30 min after which equilibrium is slowly achieved. Almost 80% of total removal for both Cu(II) and Pb(II) occurred within 60 min. The equilibrium time required for maximum removal of Cu(II) and Pb(II) were 90 and 120 min at all the experimental temperatures, respectively. As a consequence, 180 min was chosen as the reaction time required to reaching pseudo-equilibrium in the present "equilibrium" adsorption experiments. Higher removal for copper and lead ions was also observed in the higher temperature range. This was due to the increasing tendency of adsorbate ions to adsorb from the interface to the solution with increasing temperature and it is suggested that the sorption of Cu(II) and Pb(II) by MOCS may involve not only physical but also chemical sorption. The metal uptake versus time curves at different temperatures are single, smooth and continuous leading to saturation, suggesting possible monolayer coverage of Cu(II) and Pb(II) on the surface of MOCS [40].

3.6. Effect of pH on the sorption of Cu(II) and Pb(II) by MOCS

It is well known that the pH of the system is an important variable in the adsorption process. The charge of the adsorbate and the adsorbent often depends on the pH of the solution. The man-

ganese oxide surface charge is also dependent on the solution pH due to exchange of H^+ ions. The surface groups of manganese oxide are amphoteric and can function as an acid or a base [41]. The oxide surface can undergo protonation and deprotonation in response to changes in solution pH.

As shown in Fig. 8, the uptake of free ionic copper and lead depends on pH, increasing with pH from 1.4 to 5.1 for Cu(II) and 1.4 to 4.3 for Pb(II). Above these pH levels, the adsorption curves increased very slightly or tended to level out. At low pH, Cu(II) and Pb(II) removal were inhibited possibly as result of a competition between hydrogen and metal ions on the sorption sites, with an apparent preponderance of hydrogen ions. As the pH increased, the negative charge density on MOCS surface increases due to deprotonation of the metal binding sites and thus the adsorption of metal ions increased. The increase in adsorption with the decrease in H^+ ion concentration (high pH) indicates that ion exchange is one of major adsorption process. Above pH 6.0, insoluble copper or lead hydroxide starts precipitating from the solution, making true sorption studies impossible. Therefore, at these pH values, both adsorption and precipitation are the effective mechanisms to remove the Cu(II) and Pb(II) in aqueous solution. At higher pH values, Cu(II) and Pb(II) in aqueous solution convert to different hydrolysis products.

In order to understand the adsorption mechanism, the variation of pH in a solution and the metal ions adsorbed on MOCS during adsorption were measured, and the results are shown in Fig. 8. The pH of the solution at the end of experiments was observed to be decreased after adsorption by MOCS. These results indicated that the mechanism by means of which Cu(II) and Pb(II) ion was adsorbed onto MOCS perhaps involved an exchange reaction of Cu^{2+} or Pb^{2+} with H^+ on the surface and surface complex formation.

According to the principle of ion-exchange, the more metal ions that is adsorbed onto MOCS, the more hydrogen ions are released, thus the pH value was decreased. The complex reactions of Cu^{2+} and Pb^{2+} with manganese oxide may be written as follows(X = Cu, Pb and Y = Pb) [42]:

$$\equiv\mathrm{MnOH} + \mathrm{X}^{2+} \leftrightarrows \equiv\mathrm{MnO}^{-}\mathrm{X}^{2+} + \mathrm{H}^{+} \quad (9)$$

$$\equiv\mathrm{MnO}^{-} + \mathrm{X}^{2+} \leftrightarrows \equiv\mathrm{MnO}^{-}\mathrm{X}^{2+} \quad (10)$$

$$2(\equiv\mathrm{MnOH}) + \mathrm{X}^{2+} \leftrightarrows (\equiv\mathrm{MnO}^{-})_2\mathrm{X}^{2+} + 2\mathrm{H}^{+} \quad (11)$$

$$2(\equiv\mathrm{MnO}^{-}) + \mathrm{X}^{2+} \leftrightarrows (\equiv\mathrm{MnO}^{-})_2\mathrm{X}^{2+} \quad (12)$$

$$\equiv\mathrm{MnOH} + \mathrm{X}^{2+} + \mathrm{H_2O} \leftrightarrows \equiv\mathrm{MnOXOH} + 2\mathrm{H}^{+} \quad (13)$$

$$\equiv\mathrm{MnOH} + 2\mathrm{Y}^{2+} + \mathrm{H_2O} \leftrightarrows \equiv\mathrm{MnOY_2OH}^{2+} + 2\mathrm{H}^{+} \quad (14)$$

Eqs. (9)–(14) showed the hydrogen ion concentration increased with an increasing amount of Cu(II) or Pb(II) ion adsorbed on the MOCS surface.

3.7. Effect of MOCS dose

Fig. 9 shows the adsorption of Cu(II) and Pb(II) as a function of adsorbent dosage. It was observed that percent adsorption of Cu(II) and Pb(II) increased from 29 to 99% and 19 to 99% with increasing adsorbent load from 10 to 80 g l^{-1}, respectively. This was because of the availability of more and more binding sites for complexation of Cu(II) ions. On the other hand, the plot of adsorption per unit of adsorbent versus adsorbent dose revealed that the unit adsorption capacity was high at low doses and reduced at high dose. There are many factors, which can contribute to this adsorbent concentration effect. The most important factor is that adsorption sites remain unsaturated during the adsorption reaction. This is due to the fact that as the dosage of adsorbent is increased, there is less commensurate increase in adsorption resulting from the lower adsorptive capacity utilization of the adsorbent. It is readily understood that the number of available adsorption sites increases by increasing the adsorbent dose and it, therefore, results in the increase of the amount of adsorbed metal ions. The decrease in equilibrium uptake with increase in the adsorbent dose is mainly because of unsaturation of adsorption sites through the adsorption process. The corresponding linear plots of the values of percentage removal (Γ) against dose (m_s) were regressed to obtain expressions for these values in terms of the m_s parameters. This relationship is as follows:

for Cu(II):

$$\Gamma = \frac{m_s}{0.221 + 6.61 \times 10^{-3} m_s} \quad (15)$$

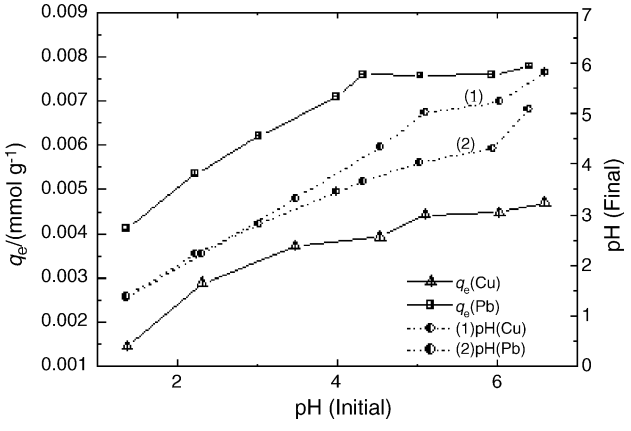

Fig. 8. Effect of pH on adsorption of Cu(II) and Pb(II) by MOCS.

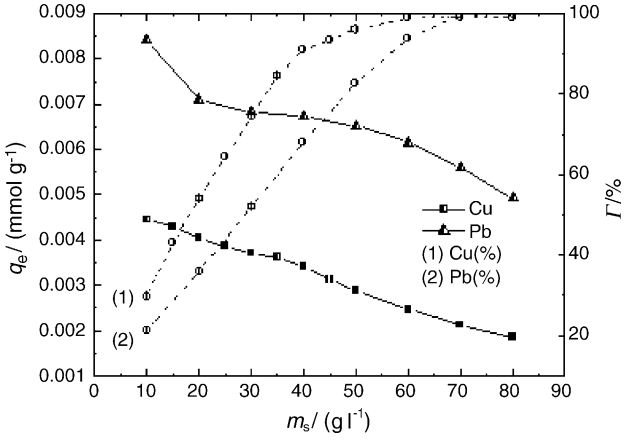

Fig. 9. Effect of dosage of MOCS on Cu(II) and Pb(II) removal.

for Pb(II):

$$\Gamma = \frac{m_s}{0.444 \times 10^{-3} + 3.85 \times 10^{-3} m_s} \quad (16)$$

These equations can be used to derive the percentage Cu(II) and Pb(II) adsorbed onto any MOCS dose within this experimental conditions due to the high values of correlation coefficient (r) of Cu(II) 0.972 and Pb(II) 0.951, respectively.

3.8. Effect of ionic strength on Cu(II) and Pb(II) adsorption

Ionic strength effects are of some importance in the study of metal ion adsorption at oxide mineral–water interfaces. It was tested by the addition of sodium nitrate and calcium nitrate to the solution of Cu(II) and Pb(II), respectively. The results of the removal of Cu(II) and Pb(II) in the presence of $NaNO_3$ or $Ca(NO_3)_2$ was shown in Fig. 10. It was seen that the increase in the salt concentration resulted in a decrease of Cu(II) and Pb(II) uptake by MOCS. This trend indicated that the binding efficiency decreased when salt concentration increased in the metal solution, which could be attributed to the competitive effect between heavy metal ions and cations from the salt for the sites available for the sorption process. The results also showed that the addition of calcium ions had a more significant influence for the sorption of Cu(II) and Pb(II) on MOCS than that of sodium ions. This could be due to the greater atomic weight and electronegativity [43]. Another factor was that increasing ionic strength resulted in the effective concentration decreasing about Cu(II) and Pb(II) and the equilibrium uptake decreased. As Ca(II) has greater contribution for ionic strength than Na(I), the effect of Ca(II) on equilibrium uptake is bigger than Na(I). Thirdly, the positive charge of Ca(II) is bigger than Na(I) and during the process of competing adsroption Ca(II) is easier to binding relative sites.

3.9. Determination of kinetic constants

In order to analyze the adsorption kinetics of Cu(II) and Pb(II) ions, four kinetic models were applied to experimental data.

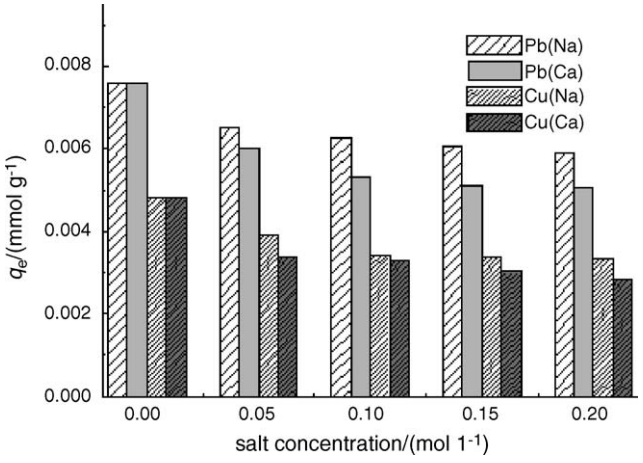

Fig. 10. Effect of salt concentration on the sorption of Cu(II) and Pb(II) by MOCS.

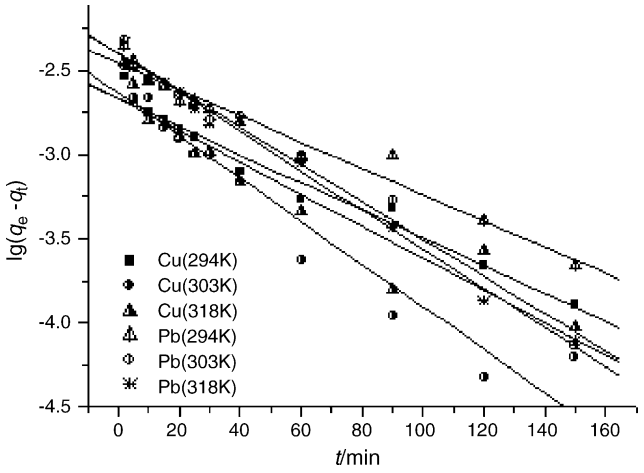

Fig. 11. Pseudo-one-order kinetic plots for the adsorption of Cu^{2+} and Pb^{2+} ions onto MOCS at various temperatures.

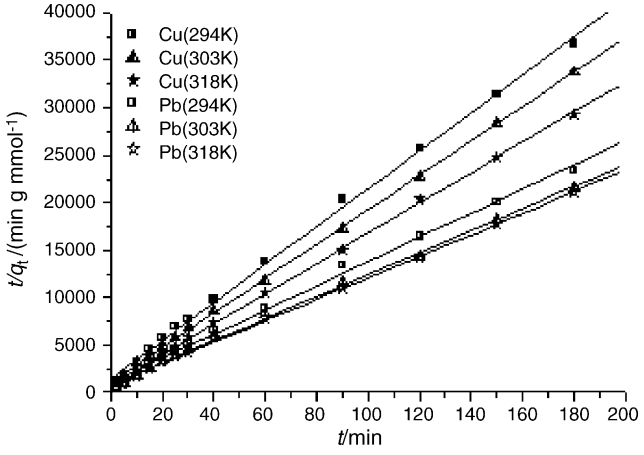

Fig. 12. Pseudo-second-order kinetic plots for the adsorption of Cu^{2+} and Pb^{2+} ions onto MOCS at various temperatures.

Figs. 11–14 show the plots of linearized form of four models at all temperature. The straight-line plots of $\log(q_e - q_t)$ versus t, t/q_t versus t, q_t versus $\ln t$, and q_t versus $t^{1/2}$ for these kinetic reaction for adsorption of Cu(II) and Pb(II) onto MOCS have

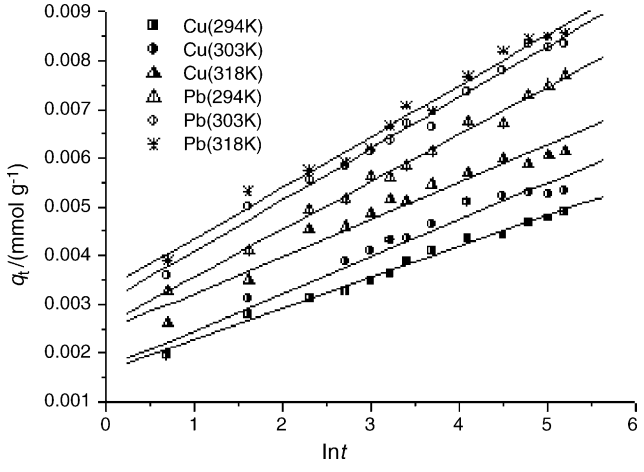

Fig. 13. Elovich equation model plots for the adsorption of Cu^{2+} and Pb^{2+} ions onto MOCS at various temperatures.

Table 2
Kinetic parameters for the adsorption of Cu^{2+} and Pb^{2+} at various temperatures by MOCS

Metal ions	T (K)	$q_{e,exp} \times 10^{-3}$	Pseudo-first-order kinetic model			Intraparticle diffusion model		
			K_1	$q_e \times 10^{-3}$	r_1	$K_t \times 10^{-4}$	$C \times 10^{-3}$	r_t
Cu^{2+}	294	4.90	0.0191	2.14	0.983	2.08	2.43	0.936
	303	5.33	0.0293	2.34	0.968	2.39	2.71	0.889
	318	6.15	0.0219	2.15	0.951	2.36	3.49	0.875
Pb^{2+}	294	7.71	0.0180	3.49	0.981	3.24	3.77	0.952
	303	8.33	0.0256	4.03	0.991	3.47	4.32	0.944
	318	8.56	0.0268	4.01	0.996	3.45	4.57	0.943

Metal ions	T (K)	Pseudo-second-order kinetic model				Elovich eqation		
		K_2	$q_e \times 10^{-3}$	$h \times 10^{-4}$	r_2	$\alpha \times 10^{-3}$	β	r_4
Cu^{2+}	294	27.3	5.00	6.83	0.999	8.55	1578	0.995
	303	29.9	5.51	9.08	1.00	7.26	1323	0.979
	318	32.0	6.26	12.5	1.00	19.7	1318	0.978
Pb^{2+}	294	15.9	7.84	.977	0.998	14.1	1029	0.996
	303	16.2	8.61	12.1	0.999	19.2	952	0.994
	318	17.0	8.83	13.3	0.999	24.9	961	0.992

also been tested to obtain the rate parameters according to Eqs. (1)–(5). Kinetic parameters for four kinetic model and correlation coefficients of Cu(II) and Pb(II) under different temperature were calculated from these plots and listed in Table 2.

The validity of these kinetic models was checked and depicted in Figs. 11–14. Among these figures, Fig. 12 showed a good agreement of dynamical data with pseudo second-order kinetic model. As shown in Table 2, the values of r_2 of pseudo second-order kinetic model for Cu(II) and Pb(II) are extremely high (>0.998) and followed by those of the Elovich equation, pseudo first-order equation and intraparticle diffusion equation, respectively (Table 2). Moreover the equilibrium sorption capacities for second-order correlation were much more reasonable when compared with experimental results than those of the first-order system because all of the equilibrium sorption capacities, q_1, of pseudo first-order were lower than experimental results. The theoretical q_2 agreed perfectly with the experimental $q_{e,exp}$ values. These suggest that the sorption systems do not follow a pseudo first-order reaction and the pseudo second-order sorption mechanism be predominant. In most cases, the pseudo first-order equation of Lagergen did not apply well throughout the whole range of contact times and is generally applicable over the initial stage of the adsorption processes. So the overall rate of the metal ions sorption process appeared to be controlled by the chemical process. For the pseudo second-order model, the rate constant and the initial sorption rate, h, increase with an increasing of temperature (Table 2). An increase in temperature results in slightly increasing the q_2. The pseudo first-order, Elovich equation and intraparticle equations do not give a good fit to the experimental data for the sorption of meatl ions. The adsorption process could be best described by the second-order equation. This suggests that the rate-limiting step may be the chemical adsorption [44].

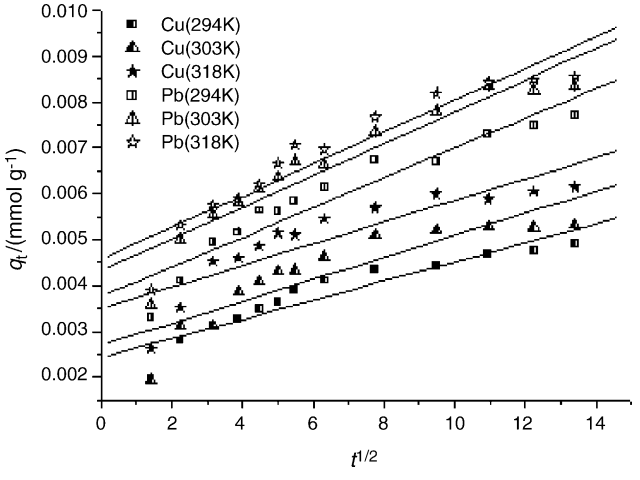

Fig. 14. Intraparticle diffusion model plots for the adsorption of Cu^{2+} and Pb^{2+} ions onto MOCS at various temperatures.

The values of rate constant from the pseudo-second-order can be used to calculate the activation energy of sorption process. The energy of activation (E_a) was determined from the slope of the Arrhenius plot of ln k_2 versus $1/T$ (figure not shown) according to Eq. (7) and was found to be 4.98 and 2.10 kJ mol^{-1} for Cu(II) and Pb(II), respectively, showing that Cu(II) and Pb(II) adsorption process by MOCS is a non-activated chemical adsorption [40], which confirm their chemical nature.

4. Conclusion

In this study, the adsorption potential of MOCS was investigated for the removal of Cu(II) and Pb(II) from aqueous systems. The kinetics of adsorption of Cu(II) and Pb(II) onto MOCS are studied at different temperature. The following results are obtained:

- The coated sand had higher specific surface area and more clusters of manganese oxide particles on the occupied surface because of the attachment of manganese oxide. SEM/EDAX analysis provides the evidence for specify adsorption of metal ions on the surface of MOCS.

- The XPS spectra indicated that the valence states of the substituted the manganese ions had a highly mixed state of Mn^{3+} and Mn^{4+}, copper and lead ions were Cu^{2+} and Pb^{+2}.
- The study of the pH effect shows that the amount of Cu(II) and Pb(II) adsorbed increases with pH and becomes insignificant for a value of pH above 5.1 and 4.3 for Cu(II) and Pb(II), respectively.
- Cu(II) and Pb(II) adsorption capacity of MOCS increase with an increasing of temperature and decrease with an increasing of salt concentrations, respectively.
- The adsorption kinetics study of the Cu(II) and Pb(II) are in accordance with the pseudo-second-order model. This indicates that the adsorption may be controlled by chemical sorption.
- It is evident that MOCS is a good sorbent for Cu(II) and Pb(II) and it can be suggested for the removal of heavy metal from wastewater. Moreover, the rapid uptake allows to consider carrying out the sorption of heavy metals on column filled with the MOCS because the contact time between the metal solution and the adsorbent is generally short in this process.

Acknowledgments

The authors express their sincere gratitude to Henan Science and Technology Department and the Education Department of Henan Province in China for the financial support of this study.

References

[1] N.K. Lazaridis, T.D. Karapantsios, D. Georgantas, Kinetic analysis for the removal of a reactive dye from aqueous solution onto hydrotalcite by adsorption, Water Res. 37 (2003) 3023–3033.
[2] Z. Al-Qodah, Adsorption of dyes using shale oil ash, Water Res. 34 (2000) 4295–4303.
[3] J.M. Zachara, P.L. Gassman, S.C. Smith, D. Taylor, Oxidation and adsorption of Co(II) $EDTA^{2-}$ complexes in subsurface materials with iron and manganese oxide grain coatings, Geochim. Cosmochim. Acta 59 (1995) 4449–4463.
[4] S.L. Lo, H.T. Jeng, C.H. Lai, Characteristics and adsorption properties of iron-coated sand, Water Sci. Technol. 35 (1997) 63–70.
[5] M.S. Al-Sewailem, E.M. Khaled, A.S. Mashhady, Retention of copper by desert sands coated with ferric hydroxides, Geoderma 89 (1999) 249–258.
[6] C.C. Fuller, J.A. Davis, J.A. Coston, E. Dixon, Characterization of metal adsorption variability in a sand and gravel aquifer, Cape Cod, Massachusetts, USA, J. Contaminant Hydrol. 22 (1996) 165–187.
[7] M. Edwards, M.M. Benjamin, Adsorption filtration using coated sand: a new approach for treatment of metal-bearing wastes, J. Water Pollut. Control Fed. 61 (1989) 1523–1533.
[8] S.L. Lo, T.Y. Chen, A growth inhibition test with sewage bacteria-results of an international ring test, Chemosphere 35 (1997) 919–930.
[9] W.H. Kuan, S.L. Lo, M.K. Wang, C.F. Lin, Removal of Se(IV) and Se(VI) from water by aluminum-oxide-coated sand, Water Res. 32 (1998) 915–923.
[10] J.J. Sansalone, S.G. Buchberger, An filtration device as a best management practice for immobilizing heavy metal in urban highway runoff, Water Sci. Technol. 32 (1995) 119–125.
[11] J.J. Sansalone, Adsorptive-infiltration of metals in urben drainage-media characteristics, Sci. Total Environ. 235 (1999) 179–188.
[12] S. Khaodhiar, M.F. Azizian, K. Osathaphan, P.E. Nelson, Copper, chromium and arsenic adsorption and equilibrium modeling in an iron-oxide-coated sand, background electrolyte system, Water Air soil Pollut. 119 (2000) 105–120.
[13] A. Joshi, M. Chaudhuri, Removal of arsenic from ground water by iron-oxide-coated sand, J. Environ. Eng. 122 (1996) 796–800.
[14] M.M. Benjamin, R.S. Sletten, R.P. Bailey, T. Bennett, Sorption and filtration of metals using iron-oxide-coated sand, Water Res. 30 (1996) 2609–2620.
[15] B.E. Reed, M. Jamil, B. Thomas, Effect of pH, empty bed contact time and hydraulic loading rate on lead removal by granular activated carbon columns, Water Environ. Res. 68 (1996) 877–882.
[16] D. Liu, Z. Teng, F.K. Cartledge, J.J. Sansalone, Surface characteristics of sorptive-filtration storm water media. I. Low-density ($\rho < 1.0$) oxide-coated buoyant media, J. Environ. Eng. 27 (2001) 866–878.
[17] D. Liu, Z. Teng, F.K. Cartledge, J.J. Sansalone, Surface characteristics of sorptive-filtration storm water media. II. Higher specific gravity ($\rho > 1.0$) oxide-coated buoyant media, J. Environ. Eng. 27 (2001) 879–888.
[18] R.P. Bailey, T. Bennett, M.M. Benjamin, Sorption onto and recovery of Cr(VI) using iron oxide-coated sand, Water Sci. Technol. 26 (1992) 1239–1244.
[19] J. Satpathi, M. Chaudhuri, Treatment of cadmium-plating and chromium-plating wastes by iron oxide coated sand, Water Environ. Res. 67 (1995) 788–790.
[20] T. Viraraghavan, K.S. Subramanian, J.A. Aruldoss, Arsenic in drinking water-problems and solutions, Water Sci. Technol. 40 (1999) 69–76.
[21] H. Green-Pedersen, N. Pind, Preparation, characterization, and sorption properties for Ni(II) of iron oxyhydroxide–montmorillonite, Colloids Surf. A: Physicochem. Eng. Aspects 168 (2000) 133–145.
[22] X. Meng, R.D. Letterman, Modeling cadmium and sulfate adsorption by $Fe(OH)_3/SiO_2$ mixed oxides, Water Res. 30 (1996) 2148–2154.
[23] X. Meng, R.D. Letterman, Modeling ion adsorption on aluminum hydroxide modified silica, Environ. Sci. Technol. 27 (1993) 1924–1929.
[24] M. Brandao, F. Galembeck, Copper, lead and zinc adsorption on MnO_2 impregnated cellulose acetate, Colloids Surf. 48 (1990) 351–362.
[25] Y. Al-Degs, M.A.M. Khraisheh, The feasibility of using diatomite and Mn-diatomite for remediation of Pb^{2+}, Cu^{2+}, and Cd^{2+} from water, Sep. Sci. Technol. 35 (2000) 2299–2310.
[26] P.B. Merkle, W.R. Knocke, D.L. Gallagher, Method for coating filter media with synthetic manganese oxide, J. Environ. Eng. 123 (1997) 642–649.
[27] P.B. Merkle, W.R. Knocke, D.L. Gallagher, J.C. Little, Dynamic model for soluble Mn^{2+} removal by oxide-coated filter media, J. Environ. Eng. 123 (1997) 650–658.
[28] P.B. Merkle, W.R. Knocke, D.L. Gallagher, J. Junta-Rosso, T. Solberg, Characterizing filter media mineral coatings, J. Am. Water Works Assoc. 88 (1996) 62–73.
[29] R.S. Stahl, B.R. James, Zinc sorption by manganese-oxide-coated sand as a function of pH, Soil Sci. Soc. Am. 55 (1991) 1291–1294.
[30] J.A. Coston, C.C. Fuller, J.A. Davis, Pb^{2+} and Zn^{2+} adsorption by a natural aluminum-and iron-bearing surface coating on an aquifer sand, Geochim. Cosmochim. Acta 59 (1995) 3535–3547.
[31] S.G. Marchetti, M.V. Cagonli, A.M. Alverez, N.G. Gallegos, J.F. Bengoa, A.A. Yeramian, R.C. Mercader, Dependence of the oxide–support interaction on the size and nature of iron oxide particles on SiO_2, J. Phys. Chem. Solids 58 (1997) 2119–2125.
[32] K.K. Panday, G. Prasad, V.N. Singh, Copper(II) removal from aqueous solutions by fly ash, Water Res. 19 (1985) 869–873.
[33] R. Selvaraj, K. Younghun, K.J. Cheol, Removal of copper from aqueous solution by aminated and protonated mesoporous aluminas: kinetics and equilibrium, J. Colloid Interf. Sci. 273 (2004) 14–21.
[34] C.W. Cheung, J.F. Porter, G. Mckay, Sorption kinetics for the removal of copper and zinc from effluents using bone char, Sep. Purif. Technol. 19 (2000) 55–64.

[35] C. Nathalie, G. Richard, D. Eric, Adsorption of Cu(II) and Pb(II) onto a grafted silica: isotherms and kinetic models, Water Res. 37 (2003) 3079–3086.

[36] C. Namasivayam, K. Ranganathan, Waste Fe(III)/Cr(III) hydroxide as adsorbent for the removal of Cr(VI) from aqueous solution and chromium plating industry wastewater, Environ. Pollut. 82 (1993) 255–261.

[37] I.A. Katsoyiannis, A.I. Zouboulis, Biological treatment of Mn(II) and Fe(II) containing groundwater: kinetic considerations and product characterization, Water Res. 38 (2004) 1922–1932.

[38] C.D. Wagner, W.M. Riggs, L.E. Davis, J.F. Moulder, G.E. Muilenberg, Handbook of X-ray Photoelectron Spectroscopy, Perkin-Elmer Corp., Eden Prairie, USA, 1979.

[39] V. Christian Taty-Costodes, H. Fauduet, C. Porte, A. Delacroix, Removal of Cd(II) and Pb(II) ions, from aqueous solutions, by adsorption onto sawdust of Pinus sylvestris, J. Hazard. Mater. B105 (2003) 121–142.

[40] Z. Aksu, Determination of the equilibrium, kinetic and thermodynamic parameters of the batch biosorption of lead(II) ions onto Chlorella vulgaris, Process Biochem. 38 (2002) 89–99.

[41] S.H.R. Davies, J.J. Morgan, Manganese (II) oxidation kinetics on metal oxide surfaces, J. Colloid Interf. Sci. 29 (1989) 63–77.

[42] P.J. Pretorius, W.L. Peter, The adsorption characteristics of δ-manganese dioxide: a collection of diffuse double layer constants for the adsorption of H^+, Cu^{2+}, Ni^{2+}, Zn^{2+}, Cd^{2+} and Pb^{2+}, Appl. Geochem. 16 (2001) 1067–1082.

[43] J. Lützenkirchen, Ionic strength effects on cation sorption to oxides: macroscopic observations and their significance in microscopic interpretation, J. Colloid Interf. Sci. 195 (1997) 149–155.

[44] F.C. Wu, R.L. Tseng, R.S. Juang, Enhanced abilities of highly swollen chitosan beads for color removal and tyrosinase immobilization, J. Hazard. Mater. B81 (2001) 167–177.